Improved Techniques for Evaluating GCM Cloudiness Applied to the NCAR CCM3

JOEL R. NORRIS

Advanced Study Program, National Center for Atmospheric Research, Boulder, Colorado*

CHRISTOPHER P. WEAVER

Department of Environmental Sciences, Rutgers—The State University of New Jersey, New Brunswick, New Jersey

(Manuscript received 17 July 2000, in final form 7 November 2000)

ABSTRACT

Evaluations of GCM cloudiness typically compare climatological output with observations, but averaging over time can obscure the presence of compensating errors. A more informative and stringent evaluation can be obtained by averaging cloud properties according to meteorological process (i.e., compositing). The present study illustrates this by comparing simulated and observed cloudiness composited on 500-mb pressure vertical velocity over the summertime midlatitude North Pacific. Observed cloud properties are daily ERBE cloud radiative forcing, daily NVAP liquid water path, and 3-hourly ISCCP cloud optical thickness and cloud-top pressure. ECMWF and NCEP–NCAR reanalyses provide vertical velocity. The GCM evaluated is the NCAR CCM3 with Rasch and Kristjánsson (1998) predicted cloud condensate. Results show that CCM3 overproduces cloud optical thickness, cloud-top height, and cloud radiative forcing under conditions of synoptic ascent and underproduces cloud cover, cloud-top height, and cloud radiative forcing under conditions of synoptic subsidence. The underproduction of cloudiness in the subsidence regime creates an unrealistic sensitivity of CCM3 low-level cloud cover to changes in circulation. As a result interannual variability of summertime midlatitude North Pacific cloudiness in CCM3 is much more closely coupled to sea level pressure variability than SST variability, opposite the case for observed cloudiness. This demonstrates small-scale cloud parameterization errors directly and dominantly impact large-scale cloud variability despite the existence of a reasonable climatology.

1. Introduction

One of the greatest uncertainties in our understanding of climate variability and climate change is the role of cloud feedbacks. Clouds have a large radiative impact on the climate system but are not correctly and consistently simulated in GCMs (Cess et al. 1996; Weare et al. 1996). The first step to improving GCM cloud parameterizations is identifying how GCM cloud properties differ from those in the real world. In-house and published evaluations of GCM cloudiness typically compare simulated and observed cloud properties using climatological and often zonal averages (e.g., Weare et al. 1996). Averaging over time has the advantage of simplicity but can obscure the presence of compensating errors. One alternative is to composite daily and hourly data over similar meteorological conditions (e.g., Tselioudis et al. 2000) to make a direct connection between cloudiness and the processes that produce it. Comparing model simulation to observations for cloud properties as a function of process more stringently evaluates the results of GCM parameterizations and provides more insight into sources of errors. Longer-term coupling between cloudiness and other parameters of the climate system can be evaluated by comparing simulated and observed correlations between monthly or seasonal cloud anomalies with anomalies in other meteorological parameters (e.g., Peterson et al. 1992).

Although these techniques can be applied to a variety of meteorological regimes, the present study focuses on cloudiness over the summertime midlatitude North Pacific. Observed cloud radiative forcing is greatest at this location and time of year (Harrison et al. 1990) so it is important that GCMs properly simulate cloud properties in this region. Large-scale midtropospheric vertical velocity is chosen as the primary process to composite over since it is the dominant dynamical mechanism creating frontal cloudiness and is documented to have a close relationship with cloud radiative forcing (Weaver and Ramanathan 1997). Cloud properties examined are cloud radiative forcing, all-sky liquid water path, and the frequency distribution of cloud optical thickness and

* The National Center for Atmospheric Research is sponsored by the National Science Foundation.

Corresponding author address: Joel R. Norris, Scripps Institution of Oceanography, University of California, San Diego, 9500 Gilman Drive DEPT 0224, La Jolla, CA 92093-0224.
E-mail: jrnorris@ucsd.edu

cloud-top pressure. These provide independent but complementary information about the quality of the cloud simulation. Daily and 3-hourly values of the cloud properties are paired with vertical velocity and averaged within vertical velocity intervals to compare how observed and simulated cloudiness responds to vertical velocity over the summertime midlatitude North Pacific. The present study also compares simulated and observed interannual covariability between summertime mean sea level pressure (SLP) anomalies and low-level cloud anomalies. It is demonstrated that problematic GCM cloud simulation on small scales directly leads to large errors in cloud–climate variability.

The GCM evaluated is the National Center for Atmospheric Research (NCAR) Community Climate Model version 3 (CCM3) with the Rasch and Kristjánsson (1998) predicted cloud condensate. Stratiform cloud fraction is diagnosed from a relative humidity scheme. Stratocumulus cloud fraction is additionally diagnosed from a scheme implementing the cloud fraction–static stability relationship documented by Klein and Hartmann (1993). Because CCM3 cannot be run in ''forecast'' mode it is not possible to evaluate the response of simulated cloudiness to the same resolved dynamical forcing experienced by the observed cloudiness (e.g., Klein and Jakob 1999; Miller et al. 1999). Instead, the observed and simulated statistical association between cloudiness and resolved dynamical forcing are compared. In this case cloud simulation errors can result from both incorrect cloud parameterization and incorrect representation of the resolved forcing. For the daily compositing study, CCM3 was run with observed monthly mean SST variations as a boundary condition and simulated output was taken from months with the same SST experienced by the observations. For the interannual variability study, output was taken from CCM3 coupled to an ocean GCM.

The first goal of this study is to document the successes and failures of cloud parameterizations in the widely used NCAR CCM, particularly those failures not readily apparent in time-average comparisons. A second goal of this study is to promote the general use of techniques that composite according to meteorological process to evaluate GCM cloudiness as a complement to time averaging.

2. Compositing data

a. Observations

Observed shortwave (SW), longwave (LW), and net (SW + LW) cloud radiative forcing (CRF) for daily mean 2.5° × 2.5° grid boxes during July 1985–89 were calculated from the Earth Radiation Budget Experiment (ERBE; Barkstrom et al. 1989) data as described in Weaver and Ramanathan (1996). It should be noted that ERBE daily means are actually calculated from a few instantaneous measurements during the day (Barkstrom 1984), and thus could include errors associated with aliasing of diurnal cloud variations. This is unlikely to produce a systematic bias because the satellite orbit precesses and values from widely separated days are averaged into the composites. Moreover, diurnal variations in cloud cover are not large over the midlatitude North Pacific (Cairns 1995; Rozendaal et al. 1995).

Observed all-sky liquid water path (LWP) values for daily mean 1° × 1° grid boxes during July 1988–92 (ocean only) were obtained from the National Aeronautics and Space Administration's (NASA) Water Vapor Project Data Set (NVAP; Randel et al. 1996). These data were retrieved from Special Sensor Microwave Imager radiances based on the method of Greenwald et al. (1993). LWP retrievals have some uncertainty, particularly in regions of precipitation, and the Greenwald et al. method produces LWP values nearly twice as large as those from Alishouse et al. (1990) and Weng and Grody (1994) but about the same as those from Petty (1990; Greenwald et al. 1993; Rasch and Kristjánsson 1998). The NVAP LWP data were averaged to 3° × 3° grid boxes, requiring all nine 1° × 1° boxes to contribute.

Observed frequencies of cloudy pixels in 42 categories for 3-hourly 2.5° × 2.5° grid boxes during July 1986 were obtained from the D1 dataset of the International Satellite Cloud Climatology Project (ISCCP; Rossow and Schiffer 1999). The categories comprise seven cloud-top pressure intervals and six cloud optical thickness intervals (daytime only). Pixels (4–7 km in size) are assumed to be completely clear or cloud filled. The presence of partial cloud cover can cause cloud optical thickness to be underestimated and cloud-top pressure to be overestimated, an effect offset by using a finite threshold for cloud detection (Rossow and Schiffer 1999). Interannual variability in LWP at constant vertical velocity was found to be much smaller than variability in LWP as a function of vertical velocity, so use of only a single year of ISCCP data should not significantly influence the results.

Large-scale vertical motion is not directly measured but can be obtained from model-dependent analyses. To provide an estimate of the uncertainties involved, results from both the European Centre for Medium-Range Weather Forecasts (ECMWF) reanalysis (Gibson et al. 1997) and the National Centers for Environmental Prediction (NCEP)/NCAR reanalysis (Kalnay et al. 1996) will be presented. Values of 500-mb pressure vertical velocity (ω) at 6-hourly 2.5° × 2.5° grid spacing were obtained for July 1985–92. ECMWF ω and NCEP ω are correlated at 0.77 over the midlatitude North Pacific, and subsequent figures will show that the composite results closely agree. The 3-hourly values of 500-mb ω were estimated by linear interpolation from the 6-hourly values. Data on the offset 2.5° × 2.5° grid of the reanalyses were interpolated using spectral methods to the 2.5° × 2.5° grid of the ERBE and ISCCP data and the 3° × 3° grid of the LWP data.

b. CCM3 simulation

The NCAR CCM3 is a global spectral model with horizontal T42 spectral resolution (approximately 2.8° × 2.8° transform grid) and 18 levels in the vertical (about four are below the 850-mb level). Further description may be found in Kiehl et al. (1998a,b), and Hack et al. (1998). The present study uses the Rasch and Kristjánsson (1998; RK) predicted cloud condensate scheme instead of the standard CCM3 diagnostic cloud condensate scheme because it will likely be incorporated into the upcoming CCM version 4. There is actually little difference between the two for the results of this study. Some additional changes made by RK include the following: 1) allowing clouds to form in the lowest layer of the model, 2) replacing the diagnostic stratocumulus cloud fraction parameterization based on Slingo (1987) with one implementing the empirical cloud fraction–static stability relationship of Klein and Hartmann (1993), and 3) removing a parameterization to diagnose ''trade cumulus'' cloudiness from shallow convective mass flux. The CCM3 parameterization diagnosing large-scale cloud fraction from relative humidity (RH) remains. This sets layer cloud fraction at a level to zero when layer RH is below the minimum RH threshold (RH_{min}) and increases cloud fraction to one when RH is 100%. The RH_{min} is 90% over the ocean and increases with increasing static stability for mid- and high-level cloudiness. Also remaining is a switch that reduces low-level cloud fraction with increasing positive ω in the model layer (cloud fraction is set to zero for $\omega > 50$ mb day^{-1}). As for the standard CCM3, liquid droplet effective size is set to 10 μm over the ocean, ice particle size increases from 10 to 30 μm between about 800 and 400 mb, and ice fraction increases from zero to one between $-10°$ and $-30°$C.

The NCAR CCM3 with RK modifications was run with observed monthly mean SST variations between 1982 and 1992 as a boundary condition. Output is daily mean or 3-hourly instantaneous on a 2.8° × 2.8° Gaussian grid. The SW, LW, and net CRF were calculated from all-sky and clear-sky top-of-model radiative fluxes. All-sky LWP was calculated by summing model layer cloud condensate discounted by ice fraction. Obtaining output suitable for comparison with ISCCP cloud category frequencies required more work. The 3-hourly instantaneous CCM3 cloud parameters for each layer in a grid box were processed to pseudosatellite data using a method based on that described in the appendix of Klein and Jakob (1999). Each grid box was divided into 100 subcolumns and cloudiness was assigned to them under the following constraints: 1) subcolumn cloud fraction is zero or one in each layer, 2) the fraction of subcolumns with cloud in a model layer is the same as gridbox cloud fraction in that layer, 3) the cloud overlap assumption is maintained (random for CCM3), and 4) subcolumn cloud is assigned the gridbox cloud optical thickness and cloud emissivity for that layer. Here 100 subcolumns were used because that is the approximate number of pixels at 30-km separation in the ISCCP 280-km equal-area grid boxes. A crude forward calculation was done to obtain IR water vapor window brightness temperature for a subcolumn, and emissivity-adjusted cloud-top pressure was then obtained from the gridbox temperature profile using ISCCP methodology (Rossow et al. 1996). Subcolumns were treated as satellite pixels and classified into the 42 ISCCP categories based on their cloud-top pressure and integrated cloud optical thickness, and frequencies of ISCCP categories were calculated for each grid box.[1]

3. Synoptic compositing

a. Analysis and results

Following Weaver and Ramanathan (1997), composite relationships between daily mean CRF and 500-mb ω over the summertime midlatitude North Pacific were constructed by matching CRF values with ω values and averaging them within ω intervals. Latitudinal weighting was applied. The ω intervals are 20 mb day^{-1} wide for $|\omega| < 80$ mb day^{-1} and become larger for large $|\omega|$ to increase sample size. At least 100 CRF values were required in an interval to contribute to the composite. Although cloud relationships have some dependence on spatial scale, no interpolation was done between the differing CCM3 and observational grids because any interpolation of nonsmooth cloud fields would likely introduce greater biases than it would remove. The 2.8° × 2.8° grid of CCM3 is judged to be sufficiently close to the 2.5° × 2.5° grid of the ERBE and ISCCP data and 3° × 3° grid of the LWP data to merit direct comparison.

Figure 1 shows SW, LW, and net CRF–ω relationships for CCM3 output and ERBE data paired with ECMWF and NCEP analyses. Here CRF is defined conventionally (Harrison et al. 1990). Both observations and CCM3 exhibit increasing SW and LW CRF with increasing ascent, but CCM3 has a steeper slope. On the other hand, CCM3 underproduces both SW and LW CRF under conditions of subsidence. The close correspondence between ECMWF and NCEP composites suggests the uncertainties in observed 500-mb ω are considerably smaller than errors in the CCM3 simulation. Note that 1/4 or less of CCM3 and observed SW and LW values overlap within extreme 500-mb ω intervals. Table 1 provides mean and quartile values of CCM3 and observed parameters under all conditions of 500-mb ω. The overproduction of SW and LW CRF by CCM3 is not the result of overly strong large-scale ascent in CCM3, as Table 1 shows that CCM3 actually has weaker

[1] To mimic the difficulty ISCCP has detecting very thin cirrus (Wylie and Menzel 1999), only subcolumns with cloud optical thickness >0.1 were identified as cloudy. Results using the nominal ISCCP threshold of 0.02 are very similar.

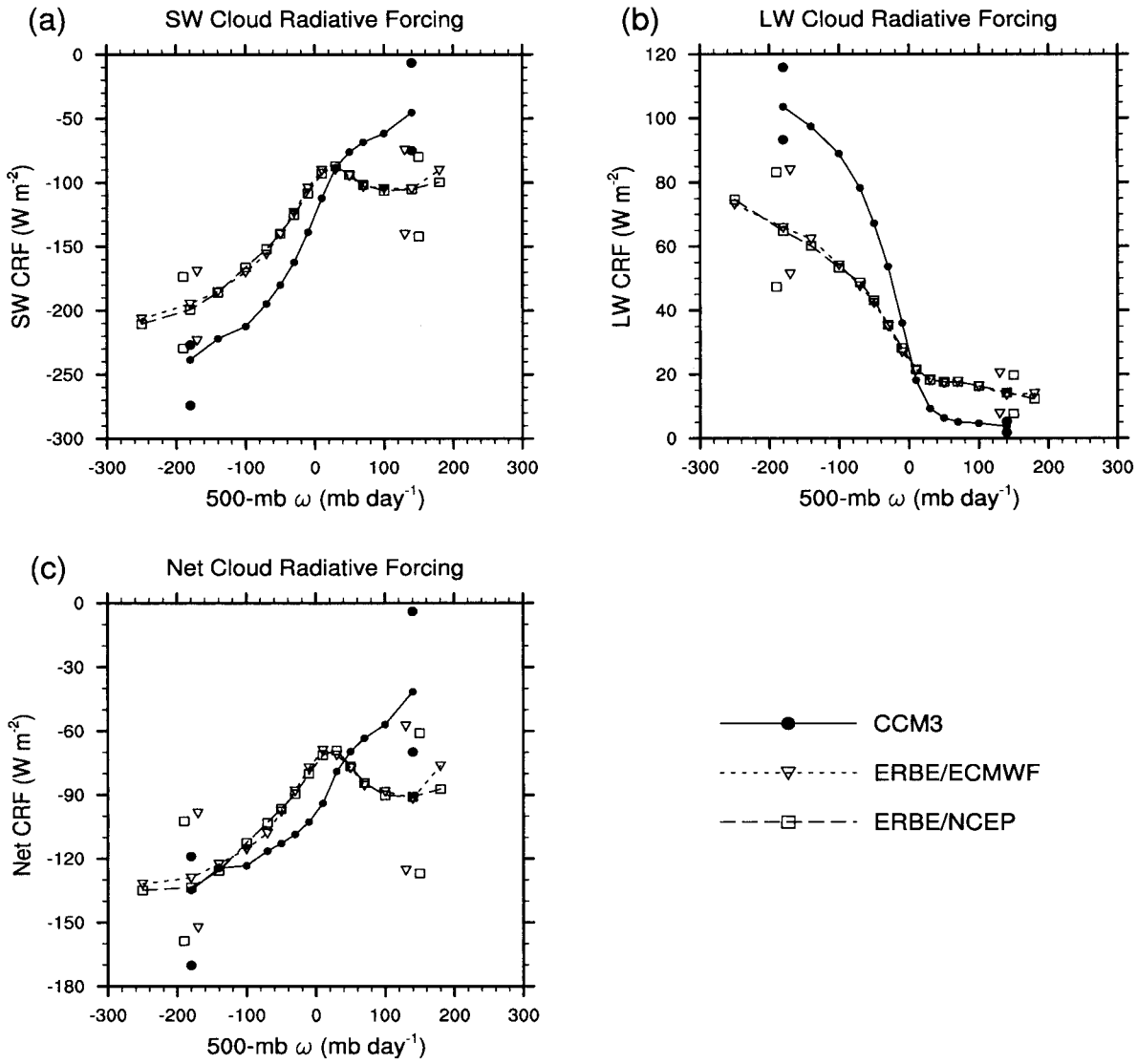

FIG. 1. Daily mean 500-mb ω (mb day^{-1}) vs (a) SW CRF (W m^{-2}), (b) LW CRF (W m^{-2}), and (c) net CRF (W m^{-2}) over the North Pacific (30°–60°N, 160°–220°E) during Jul (1985–89). Solid line and filled circles indicate CCM3 results, dotted line and open triangles indicate ERBE CRF and ECMWF ω, and dashed line and open squares indicate ERBE CRF and NCEP ω. Circles, triangles, and squares also mark the center points of the ω intervals used for averaging CRF and area-weighted upper- and lower-quartile values for CRF values within extreme ω intervals.

TABLE 1. Area-weighted mean, median, lower-, and upper-quartile values for observed and simulated daily mean parameters on 2.5° × 2.5°, 2.8° × 2.8°, or 3° × 3° grids over the North Pacific (30°–60°N, 160°–220°E) from 5 Jul.

	Mean		Lower quartile		Median		Upper quartile	
Parameter (units)	Obs	CCM3	Obs	CCM3	Obs	CCM3	Obs	CCM3
500-mb ω (mb day^{-1})*	−5, −4	−2	−34, −33	−26	4, 4	6	33, 34	29
SW CRF (W m^{-2})	−112	−126	−159	−187	−118	−133	−61	−61
LW CRF (W m^{-2})	29	32	11	5	24	17	42	55
Net CRF (W M^{-2})	−83	−94	−124	−145	−87	−101	−39	−37
LWP (mm)	0.14	0.12	0.07	0.03	0.11	0.08	0.17	0.16

* order: ECMWF reanalysis, NCEP reanalysis.

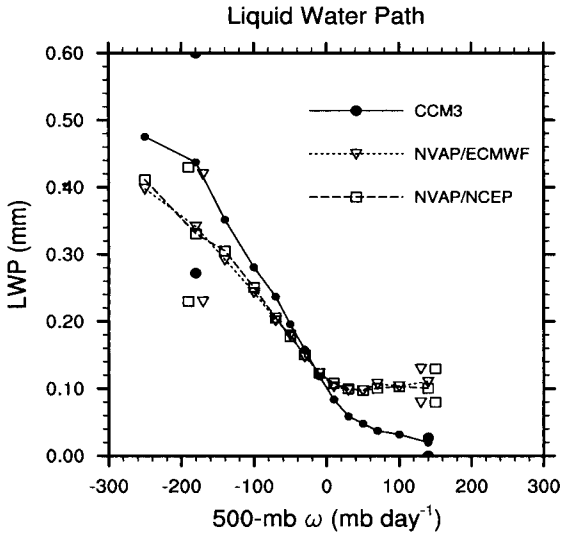

FIG. 2. As in Fig. 1, except for CCM3 and NVAP all-sky LWP (mm) during Jul (1988–92).

vertical motion than the reanalyses but more extreme SW and LW CRF values. Because the ascent regime and subsidence regime errors tend to cancel, the presence of a cloud simulation problem is not so apparent in the long-term mean. Composites constructed for the summertime midlatitude North Atlantic exhibit similar features (not shown).

The primary factors impacting SW CRF are the amount and distribution of cloud condensate and the effective particle size. To examine the role of condensate, all-sky LWP was composited on 500-mb ω in the same manner as for CRF (Fig. 2). To the extent that the observed LWP values are accurate, Fig. 2 suggests CCM3 underproduces SW CRF in the subsidence regime because it underproduces cloud condensate. With all-sky LWP alone it is not possible to determine the relative contributions of errors in cloud-only LWP and errors in cloud fraction, but Fig. 3 indicates the underproduction of cloud fraction dominates and causes the underproduction of SW CRF.

The overproduction of SW CRF in the ascent regime may also result from problems with ice water path and/or effective particle size, both of which are poorly constrained by observations. Observational studies suggest liquid water droplet effective radius is 12–14 μm (Han et al. 1994) or 11 μm (Greenwald et al. 1995) over the summertime North Pacific, but CCM3 uses a value of 10 μm. This would contribute about a 30% overproduction of SW CRF in CCM3 since SW CRF is inversely related to particle size.

The frequency distribution of cloud optical thickness and cloud-top pressure in CCM3 can be evaluated using ISCCP data (e.g., Tselioudis et al. 2000). Figure 3a displays CCM3 and ISCCP average cloud frequency distributions for the summertime midlatitude North Pacific. Unlike observed cloudiness, CCM3 cloudiness has a bimodal distribution: large optical thickness clouds with tops in the upper troposphere and medium optical thickness clouds near the surface. This bimodal distribution reflects the strong sensitivity of CCM3 cloudiness to large-scale ascent and subsidence. Figures 3b and 3c present CCM3 and ISCCP cloud frequency distributions averaged over 500-mb $\omega < -40$ mb day^{-1} and 500-mb $\omega > 40$ mb day^{-1}. Observed ω is obtained from the ECMWF reanalysis, but NCEP results are very similar. Figure 3b indicates that the CCM3 overproduction of SW and LW CRF in the ascent regime results from a frontal cloud shield that is optically too thick, too high in the atmosphere, and horizontally too extensive. Figure 3c indicates that the CCM3 underproduction of SW CRF in the subsidence regime results from insufficient cloud cover despite the greater optical thickness. Because the overproduction of CCM3 optical thickness is greater than the 30% expected from the lesser effective droplet size, greater cloud-only LWP probably also contributes. In addition to insufficient cloud cover, the excessively low height of CCM3 cloud tops could also contribute to the underproduction of LW CRF in the subsidence regime.[2]

b. Attribution of simulation errors

Although not apparent in Fig. 3, which shows only locations of cloud top, CCM3 in the ascent regime tends to fill the grid column from surface to tropopause with cloud. On the other hand, observed cloudiness in the ascent regime exhibits a variety of cloud tops and cloud vertical thicknesses (as inferred from optical thickness). CCM3 fills nearly the entire grid column with cloudiness because nearly the entire grid column becomes saturated, the result of large-scale ascent throughout the troposphere. Examination of CCM and reanalysis vertical velocity at 300, 500, and 700 mb does not reveal significantly different vertical profiles. Although not apparent in the resolved scale of the reanalyses, smaller-scale variability in vertical motion and other fields must contribute to the heterogeneity of observed cloudiness. Thus, the overproduction of SW CRF and especially LW CRF by CCM3 in the ascent regime is linked to not resolving (or parameterizing) vertical motion on scales less than 2.8° × 2.8° (T42). This supposition is supported by higher-resolution studies of CCM that show decreasing midlatitude high-level cloud cover with increasing horizontal resolution (Kiehl and Williamson 1991). Resolved ascent becomes stronger but less frequent and does not extend so deeply through the

[2] Due to the inability of satellite-retrieved temperature profiles to resolve below-inversion temperature minima, ISCCP cloud-top pressures for below-inversion cloudiness can be underestimated by 50–80 mb (Wang et al. 1999). To mimic this effect, CCM3 cloud-top pressures in Fig. 3c were assigned by matching cloud-top temperatures to above-inversion temperatures rather than below-inversion temperatures.

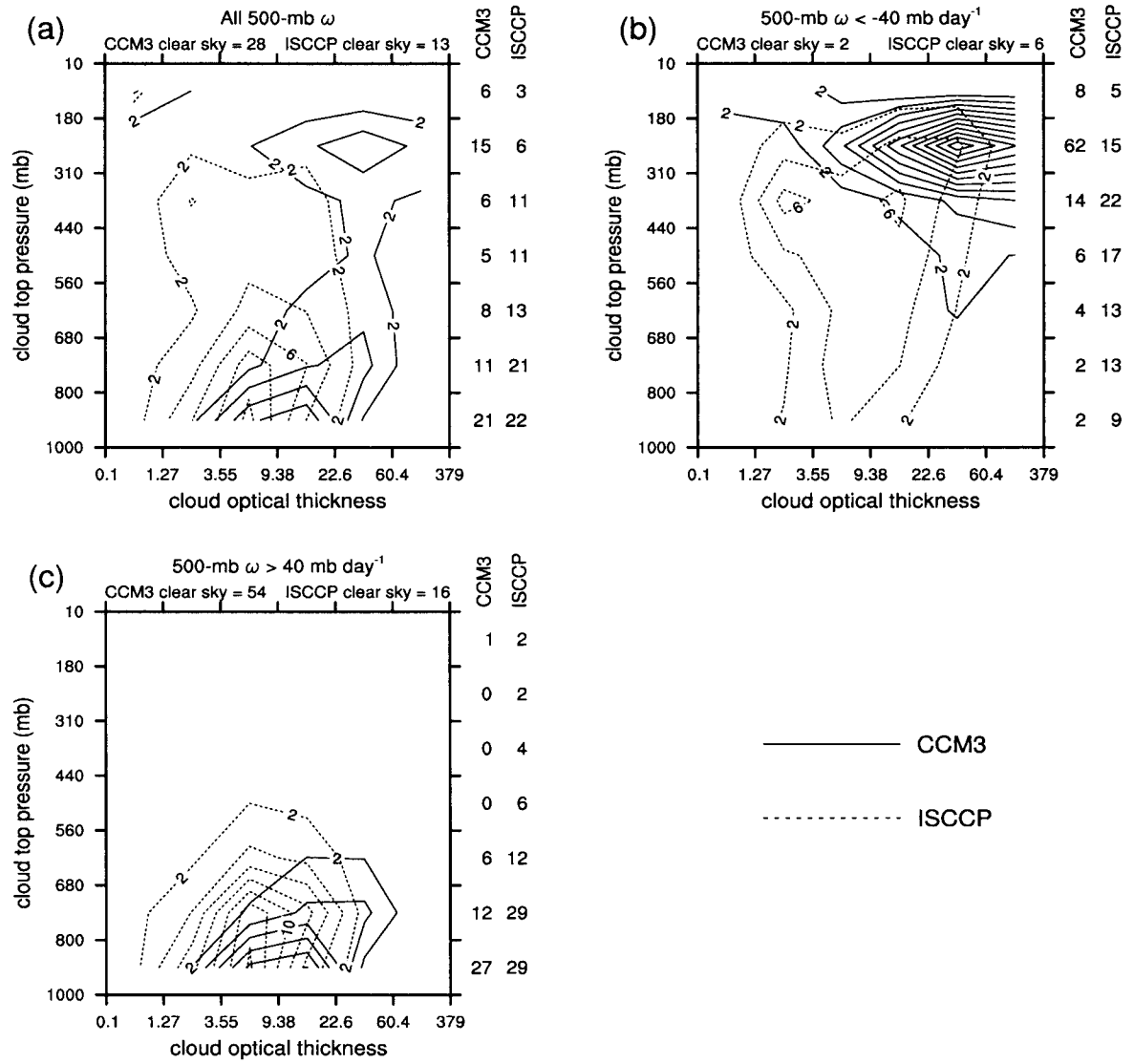

FIG. 3. Frequency distribution of cloud optical thickness–cloud-top pressure categories over the North Pacific (30°–60°N, 160°–220°E) during Jul 1986 for (a) CCM3 (solid) and ISCCP (dotted), (b) CCM3 (solid) and ISCCP–ECMWF (dotted) for 500-mb $\omega < -40$ mb day^{-1}, and (c) CCM3 (solid) and ISCCP–ECMWF (dotted) for 500-mb $\omega > 40$ mb day^{-1}. Contour interval is 2%. Numbers to the right of plots indicate cloud frequency in each cloud-top pressure category.

troposphere at higher horizontal resolutions (Williamson 1999). This would act to reduce the horizontal extent of upper-troposphere saturation and cloudiness. An attempt to account for subgrid variability in saturation is found to reduce large positive biases in midlatitude upper-tropospheric RH and cloudiness in the Hadley Centre GCM (Cusack et al. 1999).

The underproduction of mid- and high-level cloud cover in the subsidence regime by CCM is attributed to the entire drying of the free troposphere by large-scale subsidence without representation of subgrid variability. The underproduction of low-level cloud cover in the subsidence regime by CCM3 was at first attributed to the presence of the ''switch'' that set cloud cover to zero when ω in the cloud layer exceeded 50 mb day^{-1}. However, removing the switch was found to only marginally increase cloud cover. Insight into nontrivial reasons for cloud underproduction can be obtained by examining frequencies of occurrence of surface-observed low cloud-type categories associated with extreme ascent and subsidence over the summertime midlatitude North Pacific (Table 2).[3] Stratus and fog occur more often with ascent and stratocumulus and cumulus occur more often with subsidence. Hence, the underproduction of SW and LW CRF in the subsidence regime by CCM3 largely results from difficulties simulating midlatitude

[3] These were calculated by matching individual good-illumination low cloud-type observations from the EECRA (Hahn and Warren 1999) with the nearest ECMWF 2.5° × 2.5° 500-mb ω value.

TABLE 2. Frequency of occurrence of surface-observed low cloud-type categories for extreme 500-mb ω intervals over the North Pacific (30°–60°N, 160°–220°E) from Jul 1985 to 1989. Low cloud-type descriptions can be found in Norris (1998a).

Low cloud-type category	-200 mb day^{-1} $< \omega <$ -160 mb day^{-1}	120 mb day^{-1} $< \omega <$ 160 mb day^{-1}
No low cloud (C_L 0)	2%	4%
Cumulus (C_L 1, 2)	3%	10%
Cumulonimbus (C_L 3, 9)	2%	3%
Stratocumulus (C_L 4, 5, 8)	23%	46%
Stratus (C_L 6, 7)	40%	27%
Sky-obscuring fog and precipitation	31%	10%

TABLE 3. Observed and CCM3 average low-level cloud cover for surface wind direction categories over the North Pacific (30°–60°N, 160°–220°E) from Jul 1985 to 1989.

Wind from quadrant	Low-level cloud cover	
	Surface observed*	CCM3**
NE	84%	45%
SE	85%	64%
SW	86%	84%
NW	85%	64%

* From coincident individual surface observations of low-level cloud cover and wind direction.

** From CCM3 gridbox low-level cloud cover and lowest-layer wind direction.

stratocumulus. These difficulties are probably related to those responsible for the well-known and long-standing poor simulation of subtropical stratocumulus by GCMs. Both midlatitude and subtropical stratocumulus occur in inversion-capped boundary layers (Norris 1998a) where correct parameterization of unresolved processes of cloud-top radiative cooling, entrainment, turbulence, and convection is critical. CCM3 in particular and other GCMs in general (e.g., Bushell and Martin 1999) incorrectly represent the impact of these closely coupled processes on the mixing of moisture, in part due to insufficient vertical resolution, leading to overly shallow cloudy boundary layers and inability to sustain clouds in deeper boundary layers. Table 3 provides another view of CCM3 low-level cloud problems. Unlike observed low-level cloud cover from the Extended Edited Cloud Report Archive (EECRA; Hahn and Warren 1999), CCM3 low-level cloud cover[4] substantially varies with near-surface wind direction. The cloud-cover deficit occurs for wind directions often associated with inversion-capped stratocumulus boundary layers instead of the southwesterly flow associated with stratus and fog (Norris and Klein 2000; Weaver 1999). Stronger northeasterly flow is associated with even less cloud cover and stronger southwesterly flow is associated with even more cloud cover (not shown).

4. Interannual covariability

The CCM3 low-level cloud problem exhibited by Table 3 directly impacts both the climatological distribution of low-level cloudiness and interannual covariability between low-level cloudiness and other climate parameters over the summertime North Pacific. Figure 4 presents June–July–August (JJA) climatological low-level cloud cover and SLP from CCM3 coupled to an ocean GCM[5] and from observations described in Norris (2000). CCM3 particularly underproduces low-level cloudiness in the eastern North Pacific where climatological surface flow is northerly and stratocumulus predominates (Norris 1998b). Interannual covariability of JJA anomalies is explored by applying the analysis procedure and midlatitude spatial domain of Norris (2000) to CCM3 output and comparing the results. Empirical Orthogonal Function (EOF) and Singular Value Decomposition (SVD) analyses are used to identify dominant coupled spatial patterns in 44 yr of observed low-level stratiform cloud cover, SST, SLP, and storm track[6] anomalies and 38 yr of essentially equivalent output from CCM3 coupled to an ocean GCM. Specific details of the procedures may be found in Norris (2000).

Figure 5 presents the spatial patterns of the leading SVD mode for CCM3 low-level cloud paired with SLP. Over the central North Pacific summertime mean low-level cloud cover increases where surface wind anomalies are southwesterly and decreases where surface wind anomalies are northeasterly. This relationship is not apparent in the observations (Fig. 6), where the SLP pattern associated with midlatitude low-level cloud variability is very weak and not statistically significant. One measure of coupling strength is the correlation between SVD pairs of expansion coefficient time series, and Table 4 shows that low-level cloud variations are much more related to SLP variations in CCM3 than in the observations. This is not merely an artifact of the SVD analysis; correlations between EOF time series calculated independently for each parameter also show low-level cloud–SLP coupling is much stronger in CCM3 (Table 5). On the other hand, coupling between low-level cloud cover and SST is much stronger in the observations than in CCM3 (spatial patterns not shown). CCM3 underproduction of stratocumulus causes an excessive sensitivity of low-level cloudiness to changes in summertime circulation that overwhelms the observed sensitivity of low-level cloudiness to changes in SST. In the real world, variability in midlatitude low-level cloud cover primarily results from modification of

[4] Defined as below the 700-mb level.

[5] Two differences between this version of CCM3 and that used in the daily compositing analysis are the specification of 1870 greenhouse gas concentrations and the explicit representation of aerosol (direct effect only). At the time the work was done this was the only run available that used the RK predicted cloud condensate scheme and had multidecadal output. These differences are expected to have negligible impact on the results.

[6] JJA rms daily 500-mb pressure vertical velocity, as defined in Norris (2000).

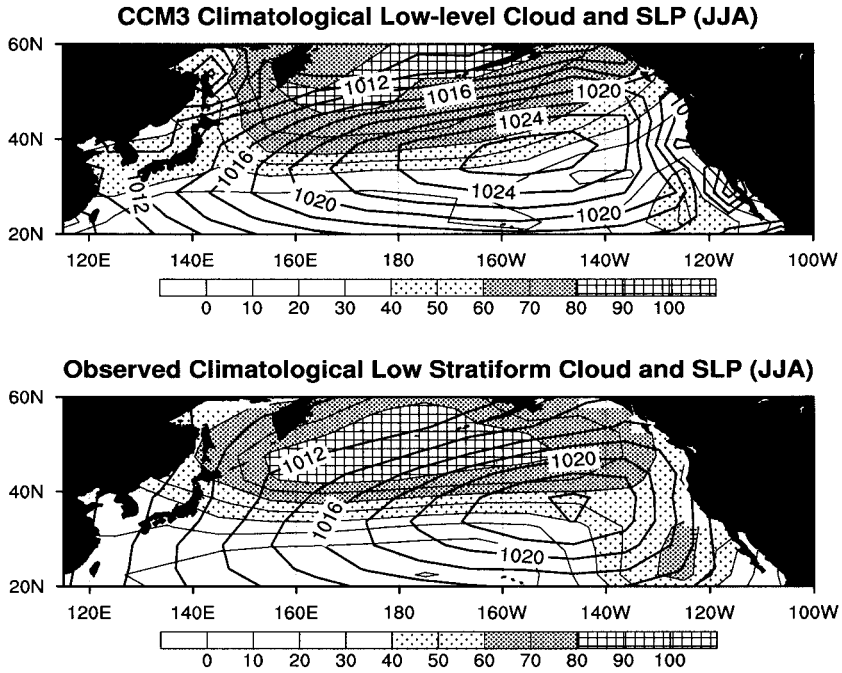

FIG. 4. Climatological JJA low-level cloud cover (thin contours and stippled) and SLP (thick contours) for CCM3 (top) and observations (bottom). Contour interval is 10% (cloud cover) and 2 mb.

the boundary layer by changes in SST (Norris et al. 1998). In the CCM3 world, variability in midlatitude low-level cloud cover primarily results from changes in the relative frequency of synoptic conditions that ought to produce inversion-capped cloudy boundary layers but often do not.

5. Conclusions

The present study introduced techniques for evaluating GCM cloudiness by comparing observed and simulated cloud properties composited on meteorological process. This approach can reveal simulation problems

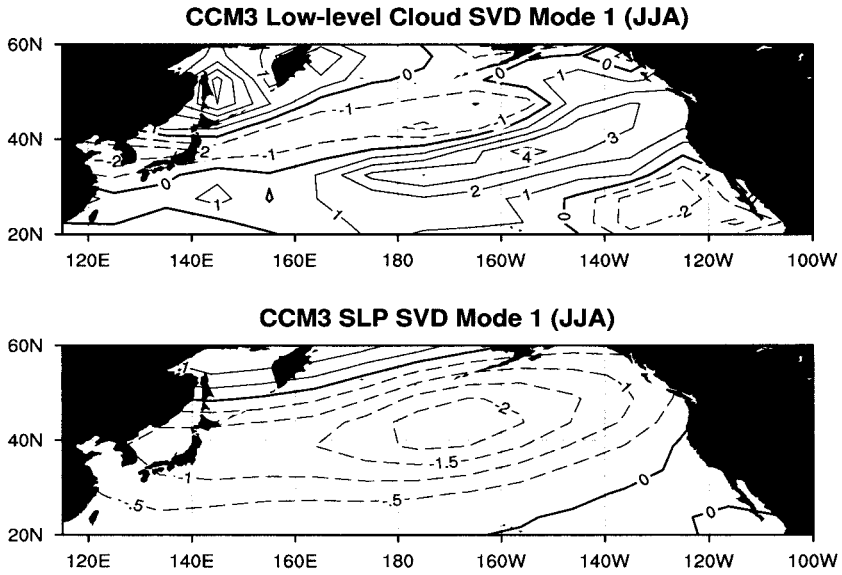

FIG. 5. Leading SVD patterns for (top) CCM3 JJA low-level cloud cover paired with (bottom) CCM3 JJA SLP. Contour intervals are 1% (cloud cover) and 0.5 mb. The zero contour is thickened and negative contours are dashed.

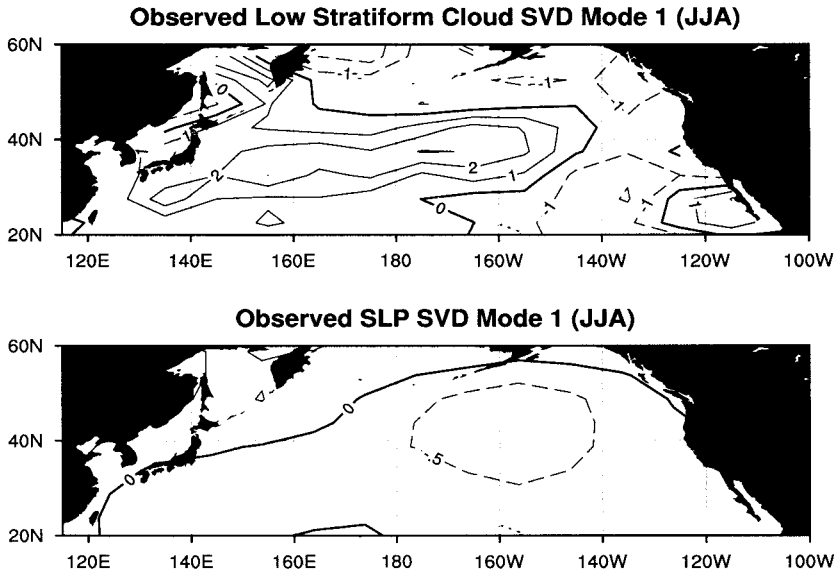

FIG. 6. As in Fig. 5 except for (top) observed JJA low stratiform cloud cover paired with (bottom) observed JJA SLP.

more effectively than comparisons of simple time and space averages, and it furthermore provides more insight into sources of errors. The performance of the NCAR CCM3 with the Rasch and Kristjánsson predicted cloud condensate was evaluated over the summertime midlatitude North Pacific using several independent and complementary cloud datasets: daily mean ERBE SW and LW CRF, daily mean NVAP LWP, and 3-hourly ISCCP cloud optical depth and cloud-top pressure. The observed variables were composited on 500-mb ω from ECMWF and NCEP–NCAR reanalyses and compared with the corresponding composites of model variables. The major result is that CCM3 overproduces cloud-top height, cloud optical thickness, and SW and LW CRF under conditions of synoptic-scale ascent, and underproduces cloud cover, cloud-top height, and SW and LW CRF under conditions of synoptic-scale subsidence. The error in the ascent regime is attributed to unrepresented subgrid variability in vertical velocity and hence saturation. The complete saturation of the tropospheric column under resolved ascent causes the CCM3 RH threshold diagnostic cloud-cover scheme to overproduce upper-tropospheric cloudiness and column-integrated condensate. Insufficient low-level cloud cover in the subsidence regime is attributed to incorrect parameterization of cloud-top radiative cooling, entrainment, turbulence, and convection. These closely coupled processes greatly affect the mixing of moisture and hence cloudiness in inversion-capped boundary layers.

The underproduction of cloudiness in the subsidence regime causes an unrealistic sensitivity of CCM3 low-level cloud cover to changes in circulation that overwhelms the observed sensitivity of midlatitude low-level cloudiness to changes in SST. As a result interannual variability of summertime midlatitude North Pacific low-level cloudiness in CCM3 is much more closely coupled to SLP variations than SST variations, opposite the case for observed cloudiness. This indicates that errors in small-scale cloud parameterizations can directly lead to incorrect cloud–climate variability even though compensation with other errors may produce reasonable climatological cloud properties. Incorrect cloud–climate feedbacks and poor simulation of climate variability and climate change may result.

The authors hope that similar compositing techniques

TABLE 4. Observed and CCM3 correlations between leading SVD expansion coefficient time series for JJA low-level cloud cover paired with other parameters. Bold indicates 95% significance. (Units: percent.)

	Low-level cloud	
	Observed	CCM3
Storm track*	**83**	**85**
SST	**87**	**74**
SLP	66	**89**

* JJA rms daily 500-mb pressure vertical velocity, as defined in Norris (2000).

TABLE 5. Observed and CCM3 correlations between pairs of leading EOF time series calculated independently for JJA low-level cloud cover and other parameters. (Units: percent.)

	Low-level cloud	
	Obs	CCM3
Storm track*	73	76
SST	71	32
SLP	34	77

* JJA rms daily 500-mb pressure vertical velocity, as defined in Norris (2000).

may be profitably applied to evaluate simulated cloudiness in other GCMs and other climate regimes. The observed composite data may be obtained by contacting the authors.

Acknowledgments. The authors thank Phil Rasch for useful discussions on CCM3 cloud parameterizations. Stephen Klein and Jonathan Vigh are also thanked for providing programs modified for use in the analysis. Bill Collins, Phil Rasch, Stephen Klein, and two anonymous reviewers also provided useful comments on the manuscript. The NVAP, ISCCP, NCEP–NCAR reanalysis, and ECMWF reanalysis data were obtained from the NCAR Mass Store. Acknowledgment is made to NCAR for the computing time used in this research. Joel Norris did this work while a postdoctoral fellow in the NCAR Advanced Study Program and the Princeton University Atmospheric and Oceanic Sciences Program. Christopher Weaver did this work while a postdoctoral associate at the Center for Clouds, Chemistry, and Climate in the Scripps Institution of Oceanography and the Rutgers University Department of Environmental Sciences and was supported by NASA Grant NAG5-9359.

REFERENCES

Alishouse, J. C., J. B. Snider, E. R. Westwater, C. T. Swift, C. S. Ruf, S. A. Snyder, J. Vongsathorn, and R. R. Ferraro, 1990: Determination of cloud liquid water content using the SSM/I. *IEEE Trans. Geosci. Remote Sens.,* **28,** 817–822.

Barkstrom, B. R., 1984: The Earth Radiation Budget Experiment (ERBE). *Bull. Amer. Meteor. Soc.,* **65,** 1170–1185.

——, E. Harrison, G. Smith, R. Green, J. Kibler, R. Cess, and the ERBE Science Team, 1989: Earth Radiation Budget Experiment (ERBE) archival and April 1985 results. *Bull. Amer. Meteor. Soc.,* **70,** 1254–1262.

Bushell, A. C., and G. M. Martin, 1999: The impact of vertical resolution upon GCM simulations of marine stratocumulus. *Climate Dyn.,* **15,** 293–318.

Cairns, B., 1995: Diurnal variations of cloud from ISCCP data. *Atmos. Res.,* **37,** 133–146.

Cess, R. D., and Coauthors, 1996: Cloud feedback in atmospheric general circulation models: An update. *J. Geophys. Res.,* **101,** 12 791–12 794.

Cusack, S., J. M. Edwards, and R. Kershaw, 1999: Estimating the subgrid variance of saturation, and its parametrization for use in a GCM cloud scheme. *Quart. J. Roy. Meteor. Soc.,* **125,** 3057–3076.

Gibson, J. K., P. Kållberg, S. Uppala, A. Hernandez, A. Nomura, and E. Serrano, 1997: ECMWF Reanalysis Project Report Series 1: ERA description. ECMWF, 72 pp. [Available from European Centre for Medium-Range Weather Forecasts, Shinfield Park, Reading, Berkshire, RG2 9AX, United Kingdom.]

Greenwald, T. J., G. L. Stephens, T. H. Vonder Haar, and D. L. Jackson, 1993: A physical retrieval of cloud liquid water over the global oceans using Special Sensor Microwave/Imager (SSM/I) observations. *J. Geophys. Res.,* **98,** 18 471–18 488.

——, ——, S. A. Christopher, and T. H. Vonder Haar, 1995: Observations of the global characteristics and regional radiative effects of marine cloud water. *J. Climate,* **8,** 2928–2946.

Hack, J. J., J. T. Kiehl, and J. W. Hurrell, 1998: The hydrologic and thermodynamic characteristics of the NCAR CCM3. *J. Climate,* **11,** 1179–1206.

Hahn, C. J., and S. G. Warren, 1999: Extended edited synoptic cloud reports from ships and land stations over the globe, 1952–1996. Carbon Dioxide Information Analysis Center, NDP026C, Oak Ridge National Laboratory, Oak Ridge, Tennessee, 71 pp. (Also available from the Data Support Section, National Center for Atmospheric Research, Boulder, CO 8030).

Han, Q., W. B. Rossow, and A. A. Lacis, 1994: Near-global survey of effective droplet radii in liquid water clouds using ISCCP data. *J. Climate,* **7,** 465–497.

Harrison, E. F., P. Minnis, B. R. Barkstrom, V. Ramanathan, R. D. Cess, and G. G. Gibson, 1990: Seasonal variation of cloud radiative forcing derived from the Earth radiation Budget Experiment. *J. Geophys. Res.,* **95,** 18 687–18 703.

Kalnay, E., and Coauthors, 1996: The NCEP/NCAR 40-Year Reanalysis Project. *Bull. Amer. Meteor. Soc.,* **77,** 437–471.

Kiehl, J. T., and D. L. Williamson, 1991: Dependence of cloud amount on horizontal resolution in the National Center for Atmospheric Research Community Climate Model. *J. Geophys. Res.,* **96,** 10 955–10 980.

——, J. J. Hack, G. B. Bonan, B. A. Boville, D. L. Williamson, and P. J. Rasch, 1998a: The National Center for Atmospheric Research Community Climate Model: CCM3. *J. Climate,* **11,** 1131–1149.

——, ——, and J. W. Hurrell, 1998b: The energy budget of the NCAR Community Climate Model: CCM3. *J. Climate,* **11,** 1151–1178.

Klein, S. A., and D. L. Hartmann, 1993: The seasonal cycle of low stratiform clouds. *J. Climate,* **6,** 1587–1606.

——, and C. Jakob, 1999: Validation and sensitivities of frontal clouds simulated by the ECMWF model. *Mon. Wea. Rev.,* **127,** 2514–2531.

Miller, S. D., G. L. Stephens, and A. C. M. Beljaars, 1999: A validation survey of the ECMWF prognostic cloud scheme using LITE. *Geophys. Res. Lett.,* **26,** 1417–1420.

Norris, J. R., 1998a: Low cloud type over the ocean from surface observations. Part I: Relationship to surface meteorology and the vertical distribution of temperature and moisture. *J. Climate,* **11,** 369–382.

——, 1998b: Low cloud type over the ocean from surface observations. Part II: Geographical and seasonal variations. *J. Climate,* **11,** 383–403.

——, 2000: Interannual and interdecadal variability in the storm track, cloudiness, and sea surface temperature over the summertime North Pacific. *J. Climate,* **13,** 422–430.

——, and S. A. Klein, 2000: Low cloud type over the ocean from surface observations. Part III: Relationship to vertical motion and the regional surface synoptic environment. *J. Climate,* **13,** 245–256.

——, Y. Zhang, and J. M. Wallace, 1998: Role of low clouds in summertime atmosphere–ocean interactions over the North Pacific. *J. Climate,* **11,** 2482–2490.

Peterson, T. C., T. P. Barnett, E. Roeckner, and T. H. Vonder Haar, 1992: An analysis of the relationship between cloud anomalies and sea surface temperature anomalies in a global circulation model. *J. Geophys. Res.,* **97,** 20 497–20 506.

Petty, G. W., 1990: On the response of the Special Sensor Microwave/Imager to the marine environment—Implications for atmospheric parameter retrievals. Ph.D. dissertation, University of Washington, 291 pp.

Randel, D. L., T. H. Vonder Haar, M. A. Ringerud, G. L. Stephens, T. J. Greenwald, and C. L. Combs, 1996: A new global water vapor dataset. *Bull. Amer. Meteor. Soc.,* **77,** 1233–1246.

Rasch, P. J., and J. E. Kristjánsson, 1998: A comparison of the CCM3 model climate using diagnosed and predicted condensate parameterizations. *J. Climate,* **11,** 1587–1614.

Rossow, W. B., and R. A. Schiffer, 1999: Advances in understanding clouds from ISCCP. *Bull. Amer. Meteor. Soc.,* **80,** 2261–2287.

——, A. W. Walker, D. E. Beuschel, and M. D. Roiter, 1996: International Satellite Cloud Climatology Project (ISCCP) documentation of new cloud datasets. WMO/TD-No. 737, World Meteorological Organization, Geneva, Switzerland, 115 pp.

Rozendaal, M. A., C. B. Leovy, and S. A. Klein, 1995: An obser-

vational study of diurnal variations of marine stratiform cloud. *J. Climate,* **8,** 1795–1809.

Slingo, J. M., 1987: The development and verification of a cloud prediction scheme for the ECMWF model. *Quart. J. Roy. Meteor. Soc.,* **113,** 899–927.

Tselioudis, G., Y. Zhang, and W. B. Rossow, 2000: Cloud and radiation variations associated with northern midlatitude low and high sea level pressure regimes. *J. Climate,* **13,** 312–327.

Wang, J., W. B. Rossow, T. Uttal, and M. Rozendaal, 1999: Variability of cloud vertical structure during ASTEX from a combination of rawinsonde, radar, ceilometer, and satellite data. *Mon. Wea. Rev.,* **127,** 2484–2502.

Weare, B. C., and AMIP modeling groups, 1996: Evaluation of the vertical structure of zonally averaged cloudiness and its variability in the Atmospheric Model Intercomparison Project. *J. Climate,* **9,** 3419–3431.

Weaver, C. P., 1999: The interactions among cyclone dynamics, vertical thermodynamic structure, and cloud radiative forcing in the North Atlantic summertime storm track. *J. Climate,* **12,** 2625–2642.

——, and V. Ramanathan, 1996: The link between summertime cloud radiative forcing and extratropical cyclones in the North Pacific. *J. Climate,* **9,** 2093–2109.

——, and ——, 1997: Relationships between large-scale vertical velocity, static stability, and cloud radiative forcing over Northern Hemisphere extratropical oceans. *J. Climate,* **10,** 2871–2887.

Weng, F., and N. Grody, 1994: Retrieval of cloud liquid water using the Special Sensor Microwave/Imager (SSM/I). *J. Geophys. Res.,* **99,** 25 535–25 551.

Williamson, D. L., 1999: Convergence of atmospheric simulations with increasing horizontal resolution and fixed forcing scales. *Tellus,* **51A,** 663–673.

Wylie, D. P., and W. P. Menzel, 1999: Eight years of high cloud statistics using HIRS. *J. Climate,* **12,** 170–184.